Supporting Information

Body-coupled-driven object-oriented natural interactive interface

Jianlong Hong, Yukun Xiao, Yuqi Chen, Shengshun Duan, Shengxin Xiang, Xiao Wei, Huiyun Zhang, Lei Liu, Jun Xia, Wei Lei, Qiongfeng Shi, Chengkuo Lee*, Jun Wu**

This PDF file includes:

Other Supplementary Materials for this manuscript include the following:

Table of Contents

Note S1: FT-IR analysis of PVC-gel with different PVC:DBA ratios.

Fourier transform infrared spectroscopy (FT-IR) is adopted to analyze the molecular interactions of pure PVC, DBA and PVC gels with different PVC:DBA ratios. It reveals that the C-Cl stretching bands of pure PVC appear at 635 cm^{-1} and 692 cm^{-1}, and the aliphatic ketone stretching band (C=O) of DBA is observed at 1732 cm^{-1}. Critically, all PVC-gel spectra display both characteristic peaks without new bond formation or peak shifts. These spectral features demonstrate that the DBA plasticizer physically disperses within the PVC polymer network rather than forming specific intermolecular bonds.

Note S2: The calculation of voltage output

For a single electrode, according to the equivalent circuit shown in Figure S6 and the Kirchhoff's voltage law, the voltage of the electrode can be described as:

$$V_{out} = V_{couple} \cdot \frac{R_{ex}}{R_{ex} + R_i + \frac{1}{jwC_d}} \tag{1}$$

Here, the capacitor between hand and interface is reckon as a parallel plate capacitor and thus we have:

$$C_d = \varepsilon \cdot \varepsilon_0 \cdot S/d \tag{2}$$

where ε is the relative dielectric constant, ε_0 is the vacuum dielectric constant of air, S is the effective area of the capacitor and d is the distance.

Substitute Equation (2) into Equation (1), we have:

$$V_{out} = V_{couple} \cdot \left(\frac{R_{ex}(R_{ex} + R_i)}{(R_{ex} + R_i)^2 + \frac{d^2}{(\varepsilon\varepsilon_0 Sw)^2}} + j\frac{R_{ex} \cdot \frac{d}{\varepsilon\varepsilon_0 Sw}}{(R_{ex} + R_i)^2 + \frac{d^2}{(\varepsilon\varepsilon_0 Sw)^2}} \right) \tag{3}$$

In our experiment, the amplitude of the voltage signals is the key parameter. Therefore, the modulus of the voltage can be solved as:

$$|V_{out}| = |V_{couple}| \cdot \frac{R_{ex}}{\sqrt{(R_{ex}+R_i)^2 + \frac{d^2}{(\varepsilon\varepsilon_0 Sw)^2}}} \tag{4}$$

Note S3: The frequency resolution of EM signature recognition

To address the resolution of closely spaced frequencies, we systematically evaluated the device's ability to distinguish similar frequencies. We measured electrical signals generated by sources with minimal frequency separation. Given that fast Fourier transform algorithm (FFT) with rectangular windowing provides high frequency resolution, this method was adopted to detect the minimum distinguishable frequency interval. We used a signal generator to produce two similar signals (Amplitude: 20 V) at closely spaced frequencies within four bands: 50 Hz, 200 Hz, 1 kHz, and 10 kHz. As shown in Figure S24, the voltage signals were acquired from the OOBI at varying source distances and analyzed via Fourier transform. From the result we can see that when the signal is near 50 Hz, 5 Hz differences were resolvable with a 10 cm distance. However, when the distance achieved 20 cm, the output signal was merged with ambient 50 Hz noise. And when we increased the differences of frequencies to 15 Hz, the output signal restored discrimination at 20 cm. Higher frequencies (200 Hz, 1 kHz, 10 kHz) maintained distinction at minimal frequency differences of 2.5 Hz, 2 Hz, and 2 Hz respectively. This enhanced high-frequency resolution stems from superior signal propagation with lower attenuation and reduced susceptibility to 50 Hz mains interference (validated in Fig. 2e).

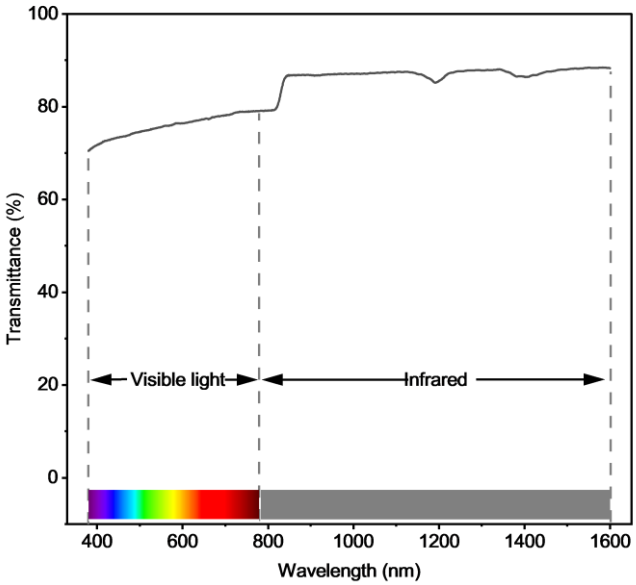

Figure S1: Transmittance of the PVC-gel with SEBS.

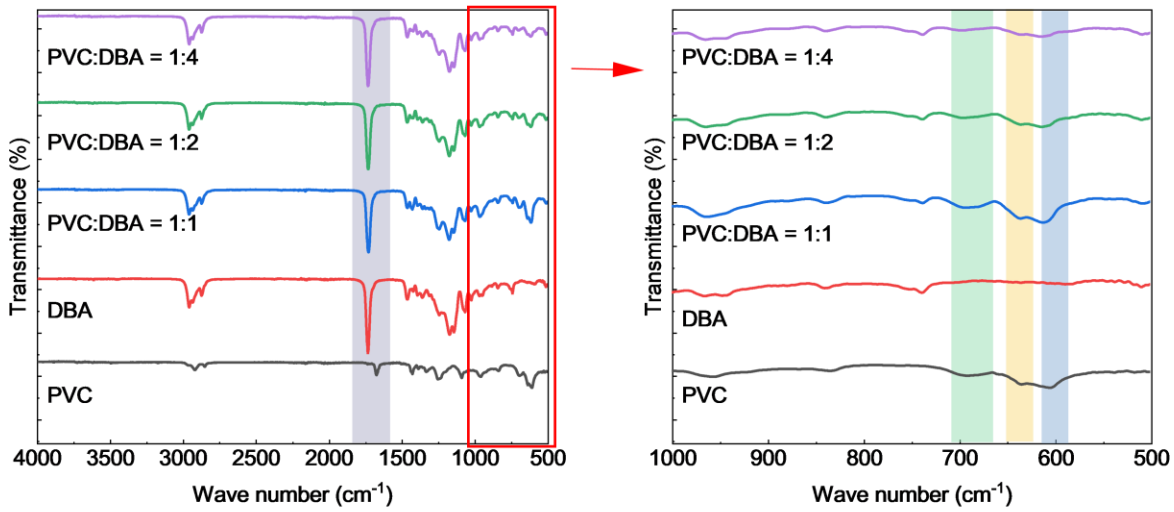

Figure S2: Fourier transform infrared spectroscopy (FT-IR) analysis of pure PVC, DBA and PVC gels with different PVC:DBA ratios (1:1, 1:2, 1:4).

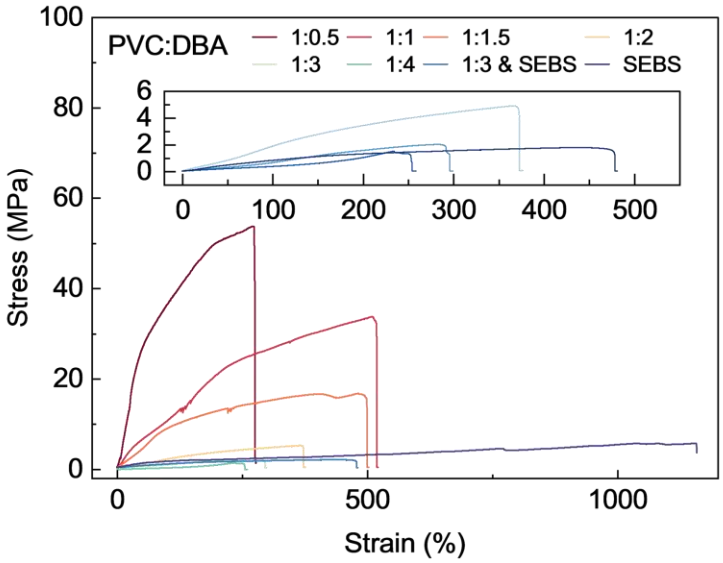

Figure S3: Stress-strain curve of fabricated membrane with different material composition ratios.

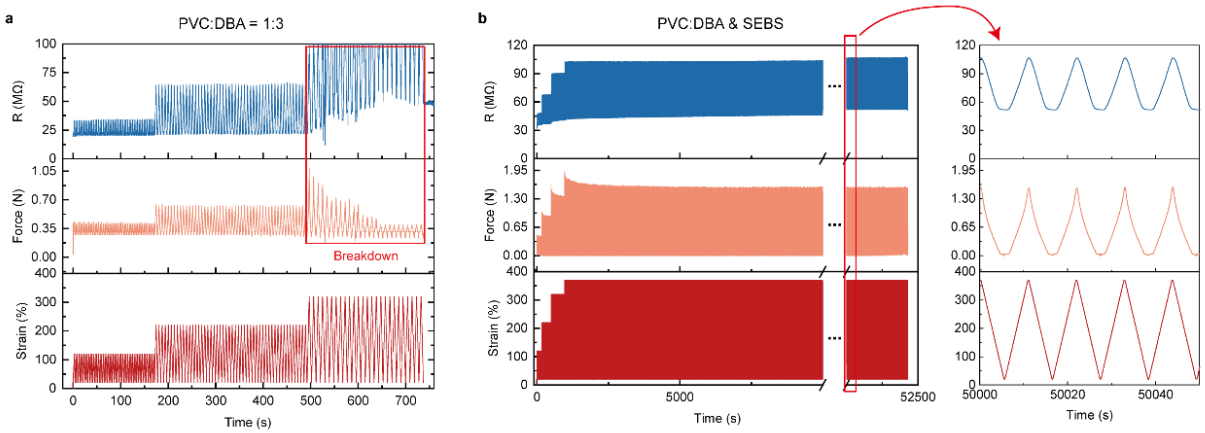

Figure S4: Comparison of the stretchability, and mechanical stability under cyclic tensile tests of PVC gels without (a) and with SEBS (b).

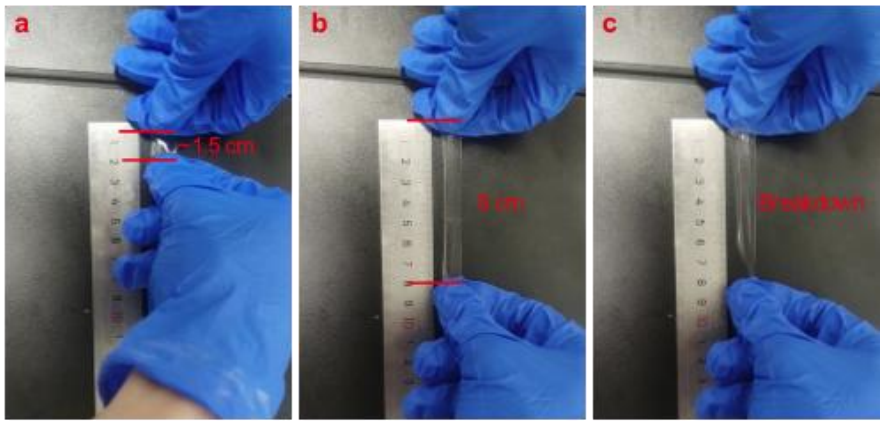

Figure S5: Stretching process of the PVC gels & SEBS.

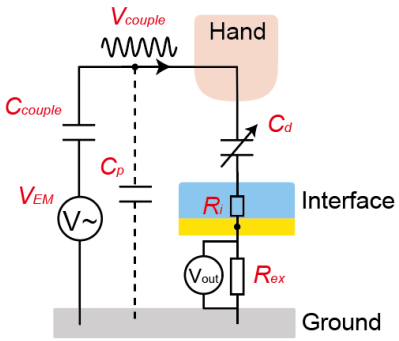

Figure S6: Simplified physical model of OOBI with a single electrode.

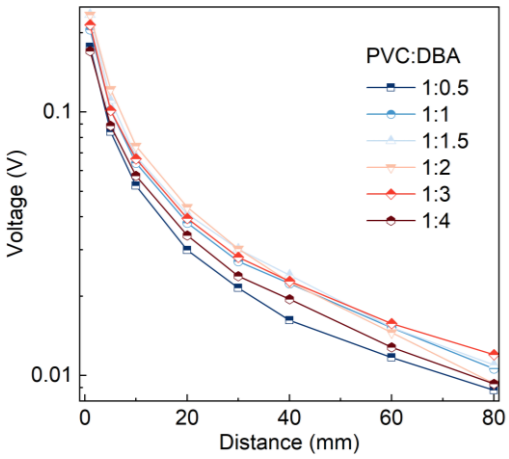

Figure S7: Voltage-distance curve of fabricated interface with different PVC and DBA ratios.

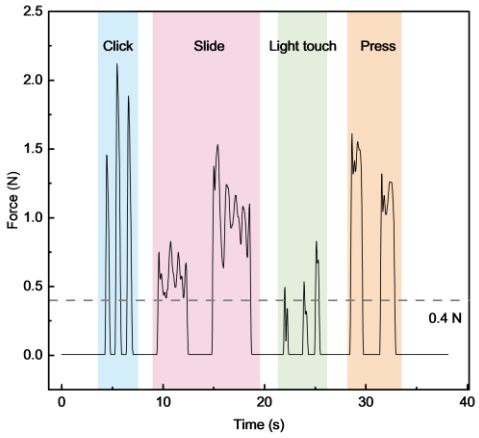

Figure S8: Applied force on the interface under click/slide/light touch/press gestures during intentional finger interactions.

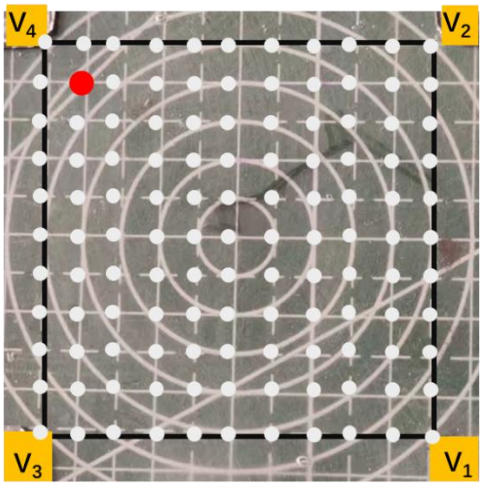

Figure S9: Illustration of touching the interface at 11 × 11 grid points.

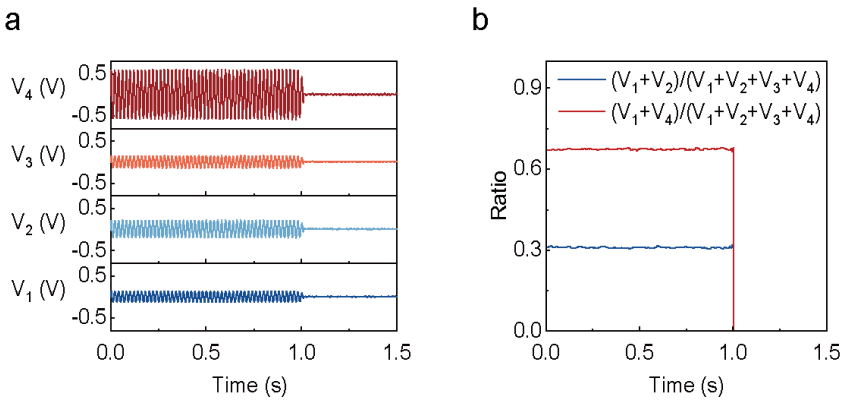

Figure S10: Output and calculated ratios when touching the interface.

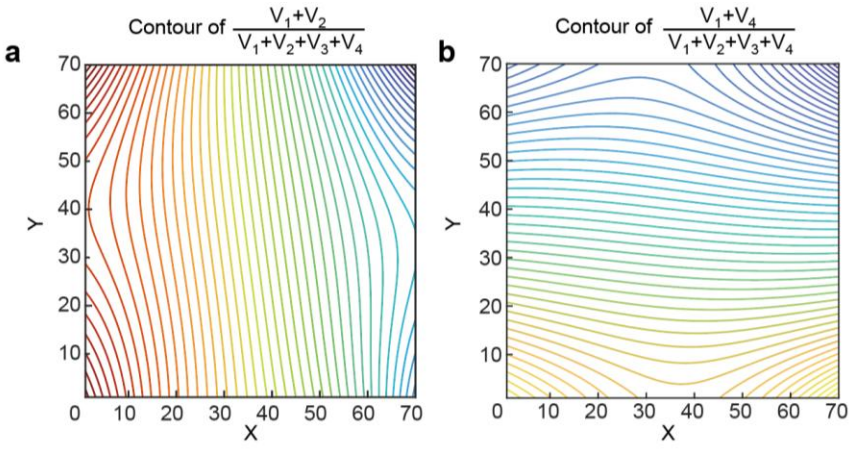

Figure S11: Isolines of two different ratios.

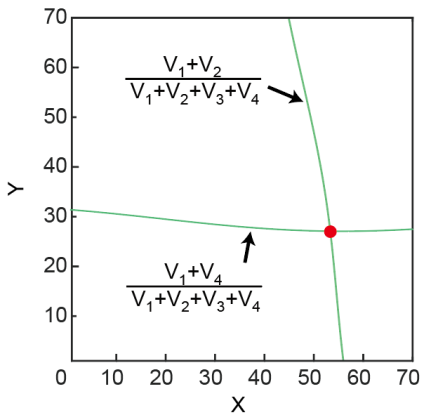

Figure S12: Intersection of two isolines from two ratios.

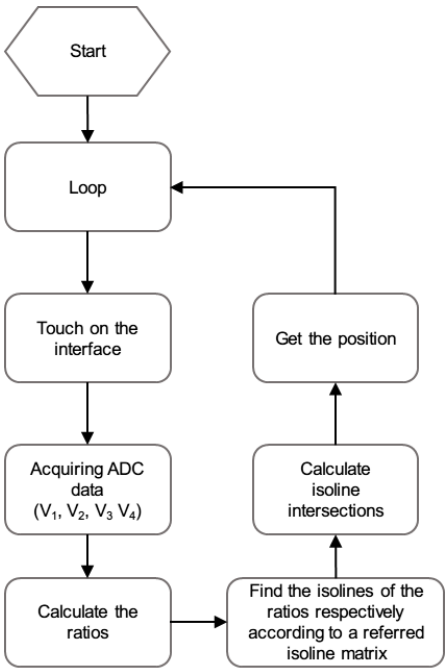

Figure S13: Flow diagram exhibiting the process to solve the touch point using isoline theory.

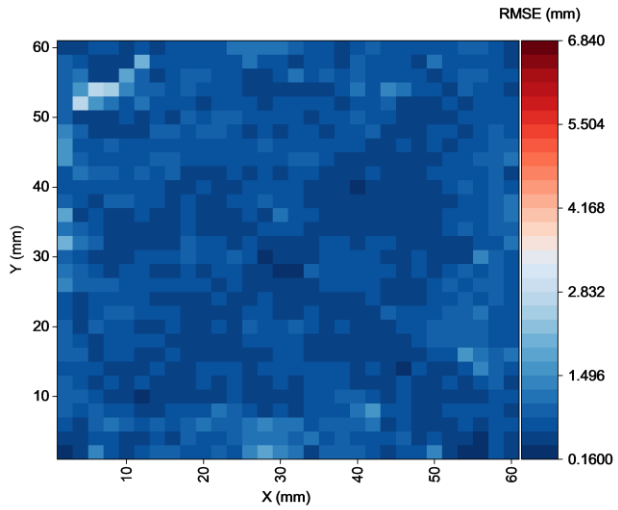

Figure S14: Distribution of positioning errors on the interface.

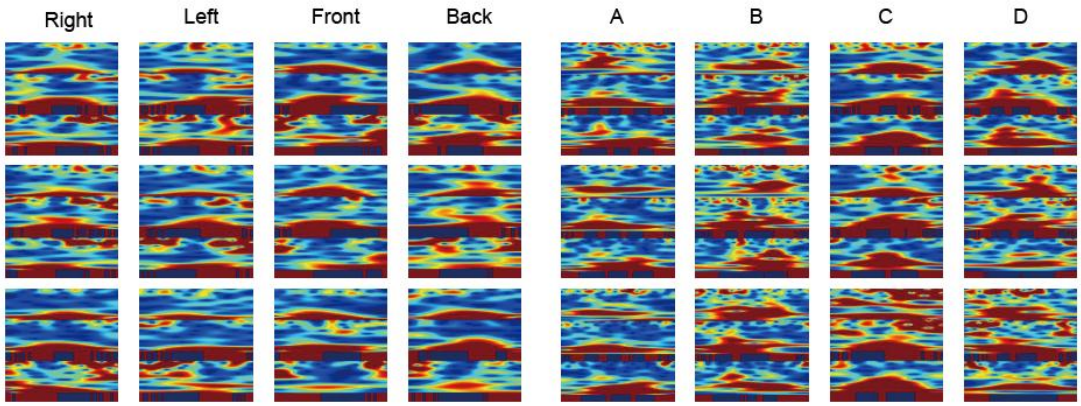

Figure S15: Samples of composite images for training and testing.

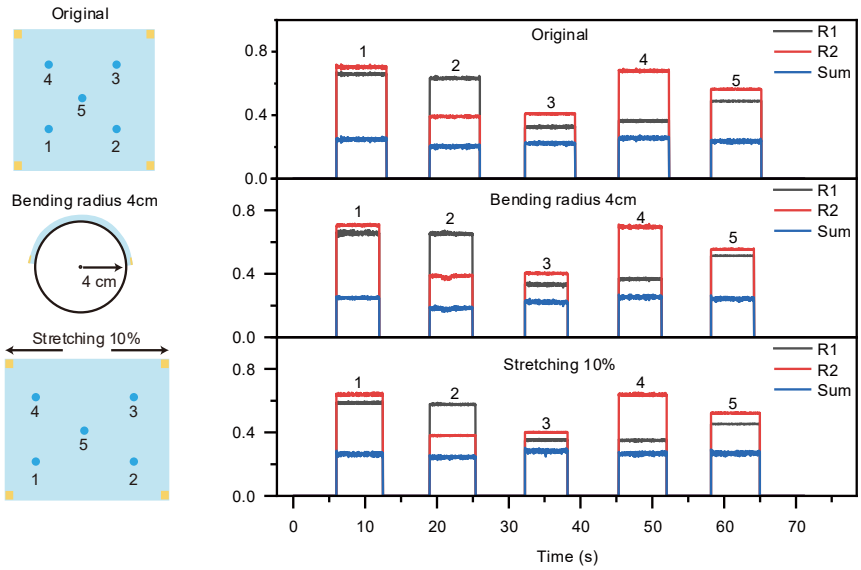

Figure S16: Variation of the three key parameters when touch the interface at 5 positions under different three states (normal state, bent state and stretched state).

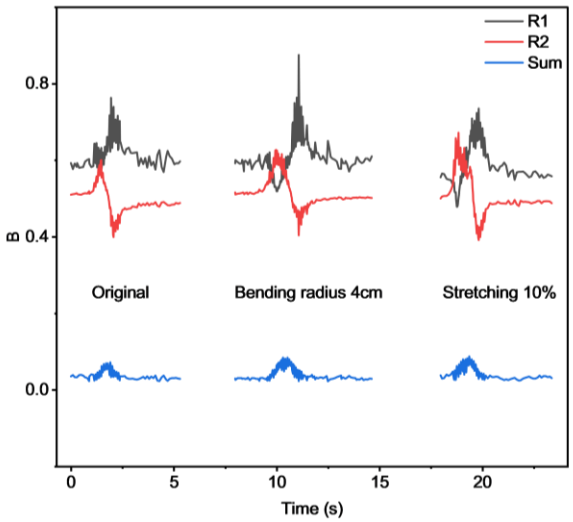

Figure S17: Variation of the three key parameters when touch the interface at 5 positions under different three states (normal state, bent state and stretched state).

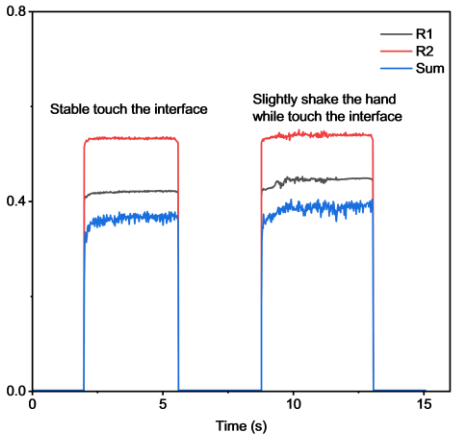

Figure S18: Variation of the three key parameters when touch the interface stably or slightly shake the hand.

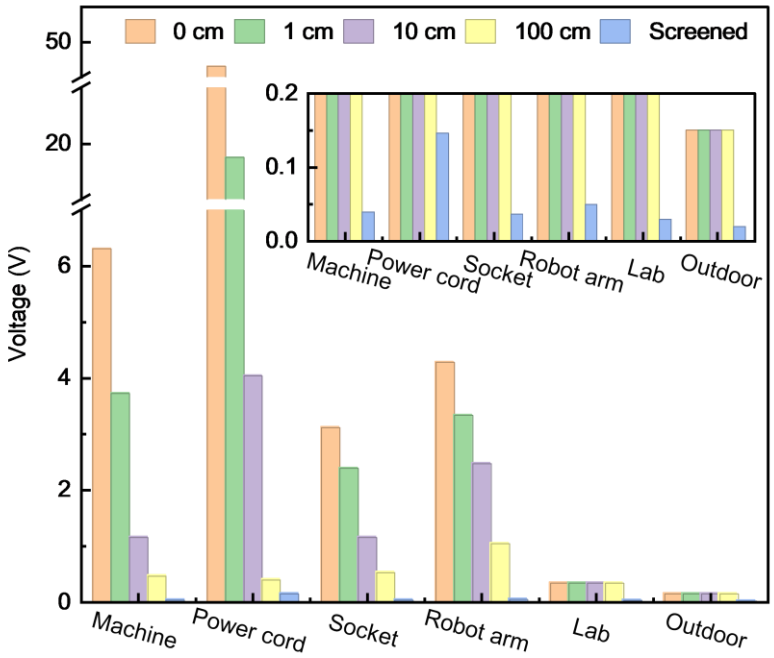

Figure S19: EM noise at different distances (orange, green, purple and yellow) from various equipment and environments. And the blue part indicates the noise output under proper shielding measures (By grounding the interface and circuitry).

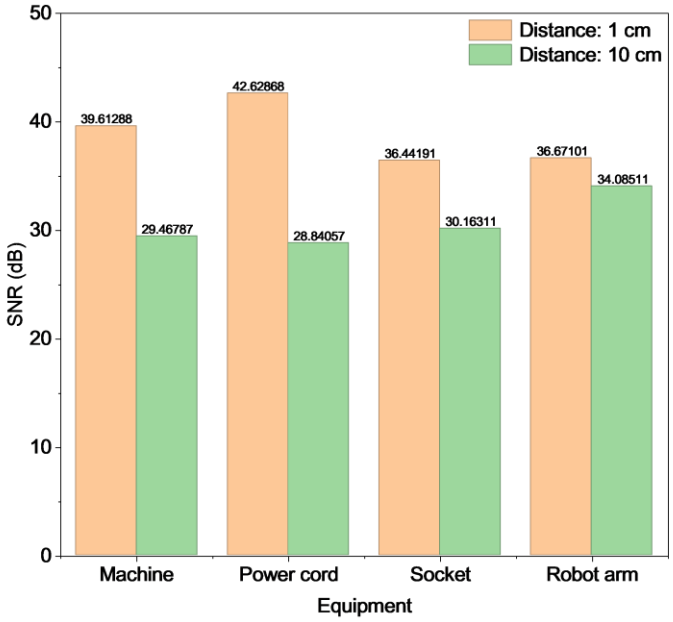

Figure S20: Calculated SNR of the interface when approaching different equipment at different distance.

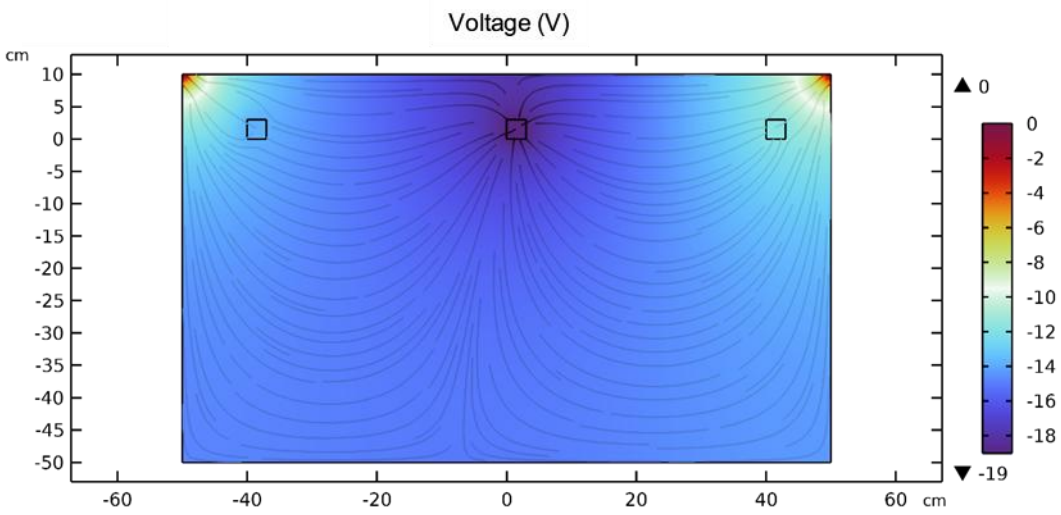

Figure S21: Experiment setting in the simulation. The details are shown in Table S2.

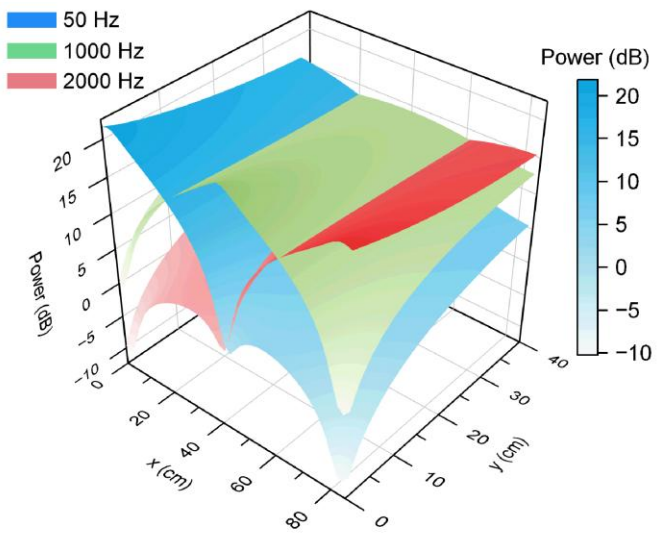

Figure S22: Spatial distribution of amplitudes from sources with different frequencies in the simulation.

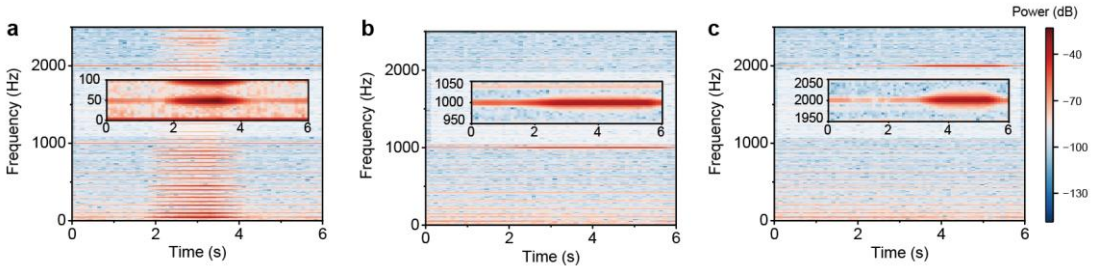

Figure S23: FFT spectrum of the signals exhibited in (a) Figure 5d, (b) Figure 5e, and (c) Figure 5f.

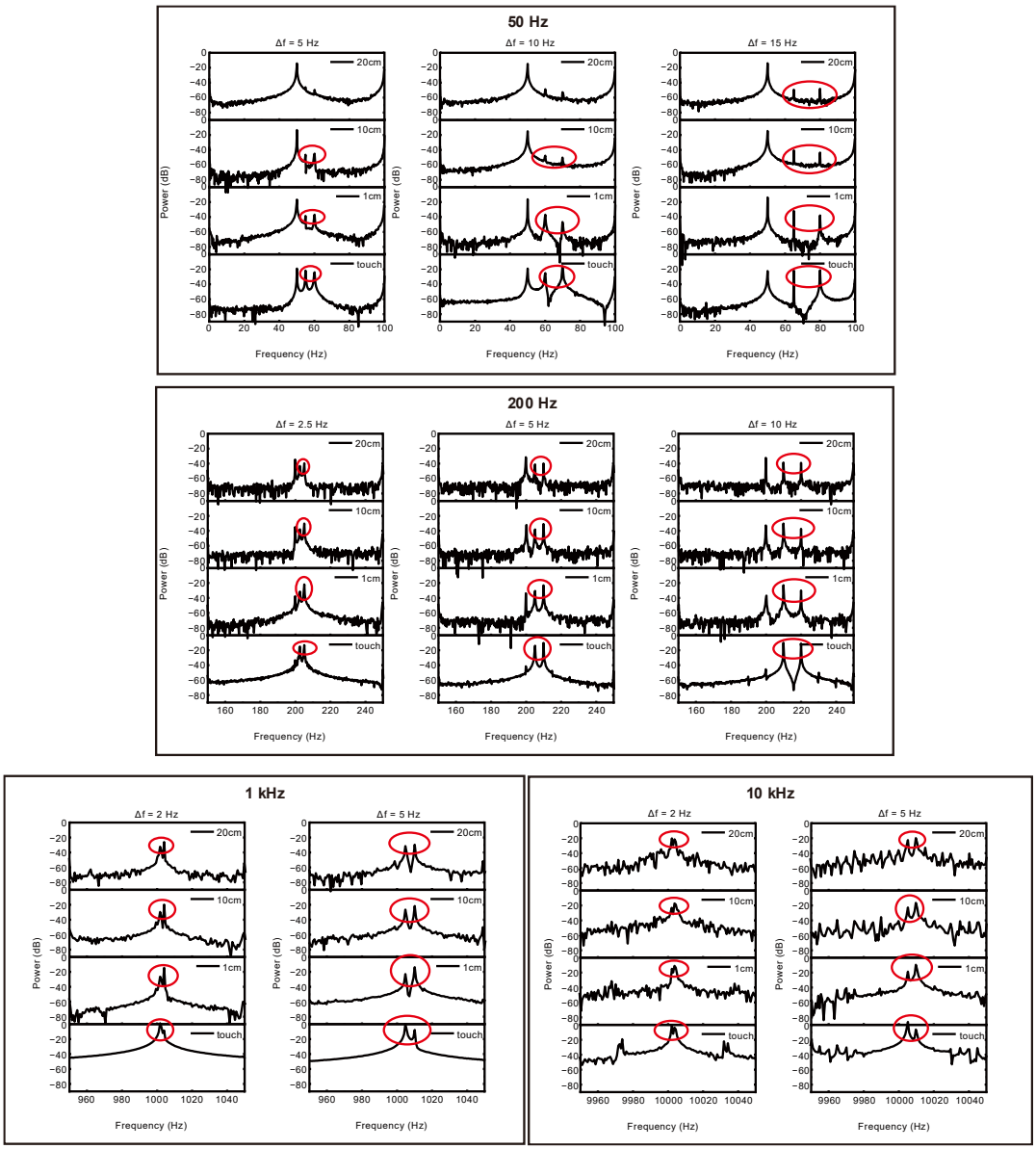

Figure S24: Fourier transform analyze the voltage of OOBI at varying distances from the source (Two similar signals produced from a signal generator; amplitude: 20 V; frequencies: closely spaced frequencies (Δ f = 2~15 Hz) within four bands: 50 Hz, 200 Hz, 1 kHz, and 10 kHz).

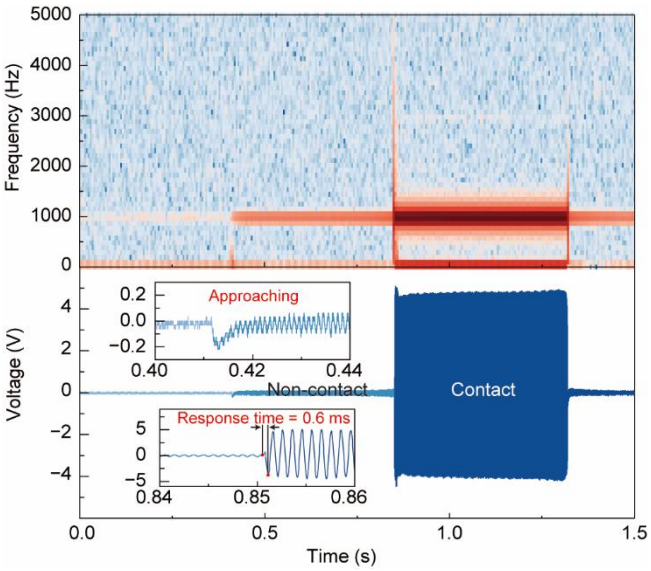

Figure S25: Voltage variation of OOBI when the finger approaching the interface under 1 kHz EM signals. The result indicates that the response time from non-contact model to contact model was about 0.6ms, which is enough to achieve seamless dual-modal switching.

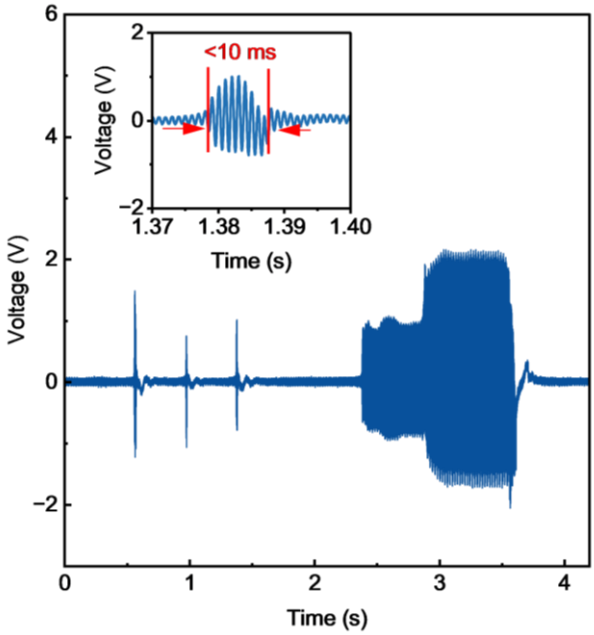

Figure S26: Dynamic response time of the OOBI. According to the result, the sensor achieved full response within 10 ms under rapid light-touch scenarios.

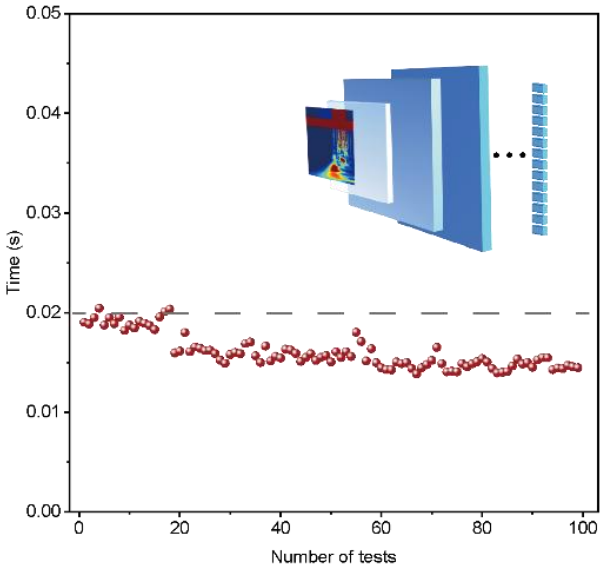

Figure S27: CNN inference time under 100 tests.

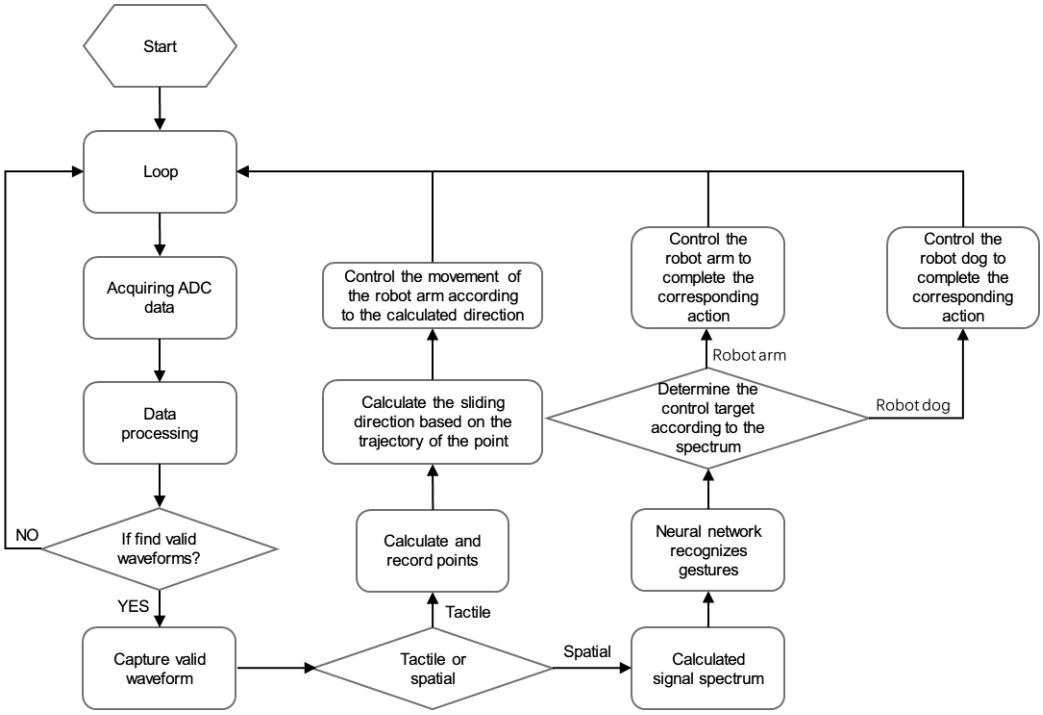

Figure S28: Control block diagram.

Table S1: Comparison of existing state of the art contactless perception e-skins

Works	Source	If self-powered	Response time (ms)	Position dimension	Position resolution (mm)	Sensing range (mm)	Tactile sensing	Force resolution, sensitivity	Mechanism	Types of gestures	If transparent	If stretchable
He et al.[1]	110 V, 2 kHz	×	400/500	3D	0.2	10	√	N/A	Humidity sensitive luminescence	N/A	×	√
Wang et al. [2]	100 kHz LCR meter	×	~300	1D	N/A	6	√	N/A, 0.93 kPa^{-1}	Capacitive	N/A	×	×
Liu et al.[3]	Contact electrification	√	N/A	1D	0.05	20	√	N/A, 0.57 Ω kPa^{-1}	Electrostatic Effect	N/A	×	√
Duan et al.[4]	Contact electrification	√	N/A	1D	N/A	12	×	N/A	Electrostatic Effect	N/A	×	×
Ge et al.[5]	DC voltage	×	<75	2D	5	N/A	√	N/A	Giant magneto-resistive sensing array	N/A	×	×
Tang et al.[6]	DC voltage	×	31	3D	>20	175	√	0.3N, 195 μA/N	Temperature sensing array	N/A	×	×
Zhu et al. [7]	Contact electrification	√	<500	3D	N/A	200	×	N/A	Electrostatic effect	N/A	×	×
Du[8]	Contact electrification	√	N/A	3D	1	70	×	N/A	Electrostatic effect	N/A	×	√
Zhou et al.[9]	100 kHz square wave	×	N/A	3D	0.005	100	√	N/A	Capacitive	N/A	√	√
Wu et al.[10]	1 MHz signal generator	×	N/A	Near 3D	N/A	40	√	N/A	Capacitive	7	√	√
Zhou et al.[11]	Contact electrification	√	N/A	3D	⩽5	250	×	N/A	Electrostatic effect Array	16	×	√
Ye et al.[12]	Contact electrification	√	50	1D	N/A	80	√	0.5 g, 19.5 MPa^{-1}	Electrostatic effect	5	×	×
This works	Multiple sources	√	<10	3D	0.2	200	√	0.05 N, 34.18 N^{-1}	Body coupled electromagnetic wave	38	√	√

Table S2: Parameters of simulation

Parameter	Value
Area of Al electrode	3×3 cm^2
Distance between Al electrodes	40 cm
Source 1	20 Vpp, 50Hz
Source 2	20 Vpp, 1000Hz
Source 3	20 Vpp, 2000Hz

Movie S1.

Demonstration of real-time calligraphy level high-resolution 2D tactile sensing.

Movie S2.

Demonstration of object-oriented interaction: object selection.

Movie S3.

Demonstration of object-oriented interaction: multi-object operation.

References

[1] J. He, R. Wei, X. Ma, W. Wu, X. Pan, J. Sun, J. Tang, Z. Xu, C. Wang, C. Pan. Contactless user-interactive sensing display for human–human and human–machine interactions. Adv Mater. **36**(25), 2401931 (2024). https://doi.org/10.1002/adma.202401931

[2] H. L. Wang, T. Chen, B. Zhang, G. Wang, X. Yang, K. Wu, Y. Wang. A dual-responsive artificial skin for tactile and touchless interfaces. Small. **19**(21), 2206830 (2023). https://doi.org/10.1002/smll.202206830

[3] W. Liu, Y. Duo, J. Liu, F. Yuan, L. Li, L. Li, G. Wang, B. Chen, S. Wang, H. Yang, Y. Liu, Y. Mo, Y. Wang, B. Fang, F. Sun, X. Ding, C. Zhang, L. Wen. Touchless interactive teaching of soft robots through flexible bimodal sensory interfaces. Nat Commun. **13**(1), 5030 (2022). https://doi.org/10.1038/s41467-022-32702-5

[4] J. Duan, G. Yue, H. Li, T. Liu, P. Wang, W. Yu, P. Shang, C. Meng, S. Guo. Self-powered noncontact triboelectric nanogenerators with microstructured square-loop surface and dielectric electron-blocking layer for far-distance motion perception and trajectory tracking. Nano Energy. **128**(109860 (2024). https://doi.org/10.1016/j.nanoen.2024.109860

[5] J. Ge, X. Wang, M. Drack, O. Volkov, M. Liang, G. S. Cañón Bermúdez, R. Illing, C. Wang, S. Zhou, J. Fassbender, M. Kaltenbrunner, D. Makarov. A bimodal soft electronic skin for tactile and touchless interaction in real time. Nat Commun. **10**(1), 4405 (2019). https://doi.org/10.1038/s41467-019-12303-5

[6] J. Tang, K. Gou, C. Wang, M. Wei, Q. Tan, G. Weng. Self‐powered and 3D printable soft sensor for human health monitoring, object recognition, and contactless hand gesture recognition. Adv Funct Mater. **34**(52), 2411172 (2024). https://doi.org/10.1002/adfm.202411172

[7] S. Zhu, Y. Li, H. Yelemulati, X. Deng, Y. Li, J. Wang, X. Li, G. Li, P. Gkoupidenis, Y. Tai. An artificial remote tactile device with 3D depth-of-field sensation. Sci Adv. **8**(43), eabo5314 (2022). https://doi.org/10.1126/sciadv.abo5314

[8] Y. Du, P. Shen, H. Liu, Y. Zhang, L. Jia, X. Pu, F. Yang, T. Ren, D. Chu, Z. Wang, D. Wei. Multi-receptor skin with highly sensitive tele-perception somatosensory. Sci Adv. **10**(37), eadp8681 (2024). https://doi.org/10.1126/sciadv.adp8681

[9] J. Zhou. Mormyroidea-inspired electronic skin for active non-contact three-dimensional tracking and sensing. Nat Commun. **15**(9875 (2024). https://doi.org/10.1038/s41467-024-54249-3

[10] W. Wu, T. Jiang, M. Wang, T. Li, Y. Song, J. Liu, Z. Wang, H. Jiang. Bioinspired monopolar controlled ionic hydrogels for flexible non‐contact human–machine interfaces. Adv Funct Mater. **34**(48), 2408338 (2024). https://doi.org/10.1002/adfm.202408338

[11] H. Zhou, W. Huang, Z. Xiao, S. Zhang, W. Li, J. Hu, T. Feng, J. Wu, P. Zhu, Y. Mao. Deep-learning-assisted noncontact gesture-recognition system for touchless human-machine interfaces. Adv Funct Mater. **32**(49), 2208271 (2022). https://doi.org/10.1002/adfm.202208271

[12] G. Ye, Q. Wu, Y. Chen, X. Wang, Z. Xiang, J. Duan, Y. Wan, P. Yang. Bimodal coupling haptic perceptron for accurate contactless gesture perception and material identification. Adv Fiber Mater. 1-13 (2024). https://doi.org/10.1007/s42765-024-00458-w